ICAST2012 #54

Wind Tunnel Testing of the Fish Bone Active Camber Morphing Concept

B. K. S. Woods[1*], O. Bilgen[2] and M. I. Friswell[1]

[1] Swansea University, College of Engineering, Singleton Park, Swansea, SA2 8PP, United Kingdom
[2] Old Dominion University, Department of Mechanical and Aerospace Engineering, Norfolk, Virginia, 23529, USA

Abstract

This work presents experimental investigations into the aerodynamic properties of the recently proposed Fish Bone Active Camber (FishBAC) morphing structure. This novel, biologically inspired, concept consists of four main elements; a compliant skeletal core, a pre-tensioned elastomeric matrix composite compliant skin, an antagonistic pair of tendons coupled to a non-backdriveable spooling pulley as the driving mechanism, and a non-morphing main spar. The FishBAC concept is capable of generating large changes in airfoil camber and is therefore proposed as a large authority, continuously variable camber solution for fixed wing aircraft, helicopters, wind turbines, tidal stream turbines, and tiltrotors. To allow for consideration of the aerodynamic performance of this concept relative to existing technology, a comparison is made between a NACA 0012 baseline airfoil with a plain trailing edge flap and the same baseline airfoil with a continuous morphing trailing edge using the FishBAC concept. Testing is performed in the low speed wind tunnel at Swansea University over a range of camber deformations and angles of attack. Both approaches are found to be able to generate similar levels of lift coefficient, however comparison of the drag results shows a significant reduction for the FishBAC geometry. Over the range of angles of attack typically used in fixed and rotary wing applications, improvements in lift efficiency on the order of 25% are realized.

1. INTRODUCTION

The amount of camber, or curvature, present in an airfoil has a significant impact on the forces it will generate under fluid flow. Fluid dynamic systems often take advantage of this fact by employing structures with variable camber. Examples of this are manifold and present in nearly every category of aerodynamic and hydrodynamic systems. Fixed wing aircraft, for example, have used camber variation to control roll, pitch, and yaw motions for over 100 years.[1] Camber variation is also used during takeoff and landing to generate very high lift coefficients.[2] Examples of helicopters employing camber change for primary control can be found as early as 1946 in the machines of Charlie Kaman.[3] Furthermore, active camber change is commonly used in hydrodynamic systems such as ship rudders,[4] submarines[5] and hydrofoil boats[6] to provide directional control.

To date, the primary means of realizing variable camber has been through the use of discrete trailing edge flaps. In this approach, the trailing edge of the airfoil structure is essentially severed then re-attached with a rotary degree of freedom. An actuation system is installed to generate torque on the flap so that it rotates up or down, thereby changing the effective camber of the foil and decreasing or increasing the amount of lift generated.

* Corresponding author, email: b.k.s.woods@swansea.ac.uk

While this approach is conceptually very simple and certainly well proven, it is not without drawbacks. First and foremost, the presence of a sharp, discrete change in camber leads to a significant increase in drag over the baseline airfoil, particularly at high lift coefficients. The sudden change in camber can also lead to early trailing edge flow separation, limiting the maximum lift coefficient. Furthermore, the flap, actuation system, and required structural reinforcements increase the weight, complexity and cost of the system.

Researchers have long pursued continuous changes to airfoil camber as an alternative due to the potential for significantly reduced drag. Additionally, arguments have been made that weight and perhaps complexity can be reduced, although this remains to be seen in practice. Many rotorcraft concepts have proposed smart material driven active camber changes, with the ambitious goals of vibration reduction, noise mitigation, and even potentially primary control.[7-9] Fixed wing examples of continuous camber change can be found throughout history,[10-12] and indeed even concepts for wind turbine blades have been explored.[13]

Much of this work has focused on the design and testing of the active camber system, without necessarily providing the direct comparison to traditional technology needed to successfully motivate the research in the first place. Part of the problem of course is that it is hard to compare a brand new concept (which is inherently far from optimal and has yet to be deployed in the field) with one that has been continuously used and perfected over one hundred years. That being said, a useful first step is to focus only on the aerodynamics and to create a direct comparison in this regard. Indeed, the entire *raison de vivre* of these structures is to generate variable aerodynamic forces, so the relative efficiency with which competing approaches do this is of primary interest. The weight, complexity, reliability, and cost that result from the specifics of the designs employed can be then considered relative to the aerodynamic benefits obtained.

To this end, the work presented here provides a direct aerodynamic comparison between a recently introduced continuously morphing active camber concept and an equivalently sized airfoil with a traditional trailing edge flap.

2. FISH BONE ACTIVE CAMBER CONCEPT

The Fish Bone Active Camber (FishBAC) morphing concept was first introduced by Woods and Friswell in 2012.[14] The FishBAC is capable of large, bidirectional changes in camber and has been proposed for use in fixed wing, helicopter, tilt-rotor, wind turbine, and tidal stream turbine applications, although it could be used anywhere else low drag camber changes are desirable. The concept combines four primary features to create a large authority, compliance based, camber morphing scheme. These are a compliant spine and stringer skeleton, pre-tensioned Elastomeric Matrix Composite (EMC) skin, an antagonistic tendon drive linked to a non-backdrivable spooling pulley, and a non-morphing, "rigid", main spar. Figure 1 provides a schematic overview of the design concept. Each feature will be briefly discussed in turn.

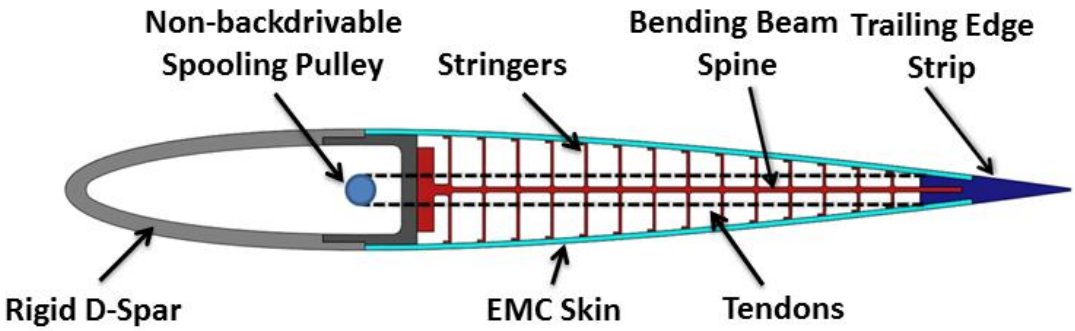

Figure 1: Fish Bone Active Camber concept diagram.

2.1. Compliant Skeleton

The core of the FishBAC concept is a compliant skeletal structure inspired by the anatomy of fish. There is a central bending beam "spine" with a series of stringers (similar to fish ribs) branching off to support the skin. This structure is designed to have high anisotropy, with a very low chordwise bending stiffness, but a high spanwise bending stiffness. This allows for camber deflections to be achieved at a low energy cost, while still allowing for global spanwise bending loads to be carried. The stringers have a dual role. They support the skin at a constant distance from the spine, thereby maintaining the thickness distribution of the airfoil during morphing and resolving the pressure loads into the structure, while also significantly increasing the spanwise bending stiffness of the skeleton structure. This compliant core is intended to be continuous along the span of the morphing portion of the wing or blade to which it is adapted. A continuous core provides the best support for the skin, thereby minimizing out-of-plane deflections due to pressure loading and deformation.

2.2. Pre-tensioned Elastomeric Matrix Composite Skin

The upper and lower skin surfaces of the morphing portion of the FishBAC concept are made from elastomeric materials. These materials are uniquely able to achieve the moderately high strains required (4-10%) without plastic deformation and with minimal energy input. This is due to their high yield strains and low moduli, respectively. Elastomers have high Poisson's ratios however, which will cause necking in at the ends of the morphing section and the development of transverse shear stresses in the bond layer between skin and structure. This can be addressed by introducing high modulus fiber reinforcement in the direction perpendicular to morphing. The high compressive stiffness of the fibers counteracts the elastomer's tendency to neck-in, creating a composite material with effectively zero Poisson's ratio. Note that this effect is primarily in-plane, so reductions in thickness of the skin still occur, although the skin thickness is such that the changes in overall airfoil thickness are very small. The concept of using EMCs for morphing aircraft is introduced in Bubert *et al*.,[15] and an equivalent concept known as Flexible Matrix Composites (FMCs) is presented in Murray, Gandhi, and Bakis.[16]

The FishBAC concept employs EMCs with one additional aspect; pre-tension. Extensile strain, and therefore tension, is applied to the skin before and during bonding to the compliant skeletal core. The reasons for pre-tension are twofold. First, if sufficient strain is applied, then the FishBAC can be designed such that the lower skin surface, which would normally be under compression, never leaves tension. This has the highly advantageous result of eliminating buckling. The thin, flexible, and only intermittently supported skins would otherwise be vulnerable to plate buckling, even with small camber deflections, with a resulting loss in smoothness of the aerodynamic surface and attendant increases in drag. Secondly, tension increases local out-of-plane stiffness. For a thin elastomeric membrane under pressure loading, out-of-plane deformations are an important design consideration. Adding tension to the skin significantly reduces deflections between stringers under a given loading without unduly increasing the weight or global stiffness of the FishBAC structure in the chordwise direction, and therefore the energy required to morph.

2.3. Non-Backdriveable Antagonistic Tendon Drive

The third feature of the FishBAC concept is an antagonistic tendon drive system coupled to a non-backdrivable spooling pulley. Two tendons are mounted symmetrically about the bending spine. One end of each tendon is anchored to the rigid portion of the trailing edge, and the other end wraps around a spooling pulley mounted inside the non-morphing spar, with each tendon spooling in opposite directions. In between the pulley and trailing edge, the tendons travel through holes in the stingers. These holes are made with diameters only slightly larger than the tendons, so that the tendon's distance from the neutral axis is essentially constant under morphing deflections. This enforces equivalent strains in the two tendons and simplifies the kinematics of the tendon drive system. Rotation of the spooling pulley creates bending moments on the trailing edge due to the tension forces in the tendons acting at the fixed offset distance from the neutral axis. This provides a symmetric means of driving the morphing deflections, allowing for bidirectional changes in camber. Bi-directionality is particularly important in rotary wing applications where both increases and decreases in lift or aerodynamic pitching moment over the baseline airfoil are desired.

A non-backdriveable mechanism is a device which cannot be driven by its load. A pertinent example is a worm and worm gear pair. Driving the worm rotates the worm gear and allows torque transmission, however attempting to drive the worm gear causes friction locking due to the low lead angle of the worm. Such a device is used in the FishBAC between the spooling pulley and the actuator, such that the actuator can drive the tendons, but not vice versa. The advantage provided by this device is that it allows for the stiffness of the tendons to contribute to the chordwise bending stiffness under external loads without increasing the amount of internal energy required to morph the airfoil. This is because external loading activates the friction locking by attempting to back-drive the mechanism, thereby allowing the stiffness of the tendons to add to the inherent structural stiffness. In this case, deflections of the structure can only be achieved through directly straining the tendons. On the other hand, internal actuation acts through the mechanism in the drivable direction, imposing deflections on one end of the tendons which drive the morphing deflections, without requiring the tendons themselves to strain. This mechanism creates a non-linearity in the stiffness of the structure which helps to address a fundamental problem present in all morphing structures; that of having sufficiently low stiffness to minimize energy requirements during morphing while simultaneously having high enough stiffness to maintain the shape once deflected. One way to conceptualize this aspect of the concept is to consider it as increasing the "external" stiffness of the structure without changing the "internal" stiffness.

Additionally, the friction locking effect allows for the morphed position to be retained with no energy input from the actuator, significantly reducing power requirements, particularly for configuration type changes in camber where a certain morphing deflection is to be maintained for a considerable period of time as a result of changes in operating conditions.

The FishBAC concept can be used with any type of actuation technology that can generate the torques and rotations required to drive the spooling pulley. Another advantage of the non-backdriveable mechanism is that the stiffness of the actuator is isolated from the stiffness of the morphing section. This allows actuators to be chosen independent of their inherent stiffness, which opens up new possibilities. For example, Pneumatic Artificial Muscles are a very promising technology because of their high specific work and use of pressurized air instead of hydraulic oil.[17] The reduced stiffness of these actuators relative to a hydraulic cylinder, which may be a design consideration for a traditional flap, is immaterial for use in the FishBAC concept.

2.4. Non-morphing Main Spar

The FishBAC concept includes a non-morphing spar as the primary global load carrying structural element. This feature considerably increases the feasibility of the concept by allowing for traditional material and geometric solutions to be applied to carrying the large global bending, torsional, and shear loads. The configuration shown in Figure 1 has a "rigid" D-spar forming the leading edge. This approach is adopted from helicopter blades, many of which use such a D-spar as the primary structural element.[18] Since the chordwise length of the morphing section is an open design variable, shorter morphing sections could alternatively be mounted to the type of box spars often employed on fixed wing aircraft. In either case, the benefits are the same. By restricting the morphing portion to a specific region of the chord, the structure can be significantly stiffer under spanwise loading than a structure that uses the entire chord length to morph.

The use of a non-morphing main spar also provides a rigid area for mounting the actuation system, and allows for a modular morphing approach to be used. The morphing area of the wing or blade could be divided into several spanwise sections, each mounted independently to the non-morphing spar. In this manner maintainability, redundancy, and reliability of the system could be improved.

3. WIND TUNNEL EVALUATION

This section discusses the wind tunnel testing performed. The primary objective of this study is to quantify the improvements, if any, provided by the use of smooth, continuous camber change (as realized with the FishBAC concept) over traditional, discrete trailing edge flaps. If significant changes can be seen, then the concept will be worth pursuing. However, without meaningful enhancements to

the performance of the airfoil, there is little motivation to pursue alternative concepts given the simplicity and efficacy of the well-established trailing edge flap technology. The evaluation conducted here therefore attempts to create a direct comparison of the two under matched operating conditions.

The development of the test articles with FishBAC and flapped geometries will first be discussed, with particular attention paid to the details of the novel FishBAC prototype. The geometry, flow parameters, and instrumentation of the wind tunnel used will then be discussed, followed by the range of test variables explored in this study. Finally, the wind tunnel blockage corrections which were applied to the raw data are presented.

3.1. FishBAC Wind Tunnel Model Construction

In order to allow for experimental aerodynamic characterization of the FishBAC concept, a wind tunnel test article was designed and built. This test article does not incorporate all four aspects of the concept in their entirety, as some simplifications were made in the interest of time. Only the aspects directly related to aerodynamic performance were included. The model therefore does not include a non-backdriveable mechanism, and a single agonist tendon is employed instead of an agonist/antagonist pair. The result of these simplifications is that the model requires constant power input to maintain a deflected position, and the morphing deflections are uni-directional. However, the actuator's consumption of a nominal 12W during testing is immaterial, and the symmetric baseline airfoil means that in principle the results for morphing deflections in one direction can be mirrored for application in the second direction. Therefore the model as built is fully able to provide the aerodynamic characterization desired. That said, the efficacy of the non-backdrivable mechanism at holding morphed position, increasing "external" stiffness and isolating actuator stiffness still needs to be verified experimentally, and work is underway now to this effect. An overview of the geometric parameters of the FishBAC prototype is presented in Table 1.

Table 1. FishBAC prototype geometric parameters

Parameter	Value
airfoil	NACA 0012 (baseline)
chord (c)	305 mm
span (b)	150 mm
start of morph (x_s)	$0.35c$ = 107 mm
end of morph (x_e)	$0.85c$ = 260 mm
spine thickness (t_b)	2 mm
# of stringer pairs	14
stringer thickness (t_{st})	0.8 mm
skin thickness (t_s)	1.5 mm
tendon offset (y_t)	4.2 mm
tendon diameter (d_t)	0.7 mm
pulley deflection angle (δ_p)	0 - 90°

The structural components of the model, with the exception of the skin, were printed from ABS plastic using an HP Designjet 3D Fused Deposition Modeling printer. The silicone matrix, unidirectional carbon fiber reinforced EMC skin was made using a multi-step laminating process which was a modified form of that presented elsewhere.[15,19]

A single tendon made of Kevlar braided cordage was anchored to the trailing edge strip on the bottom surface of the airfoil with an offset (y_t) of 4.2 mm from the center of the bending spine. This tendon was then strung through small holes (1 mm diameter) printed into the stringers at a constant center offset of 4.2 mm. The tendon then passed through the back wall of the D-Spar and wrapped eight times around an aluminum spooling pulley before being tied off to an exposed bolt anchored in the pulley. Spooling in this manner allows for gradual frictional force transfer, minimizing the tendon stress at the final mechanical anchor point and increasing strength. The spooling approach also allows for the pulley to be wound in (thereby causing camber deformation) without changing the tendon

offset. The pulley was supported by a pair of radial bearings to effectively resolve the tendon tension force into the structure with very small rotational friction losses.

The spooling pulley was directly connected to a commercial off-the-shelf brushless electric motor driven servo actuator, of the type commonly used for radio controlled aircraft. The particular unit used was a Futuba BLS157HV High Voltage Ultra Torque Servo, which is able to generate 3.6 N-m of torque in a compact package (21 x 54.5 x 46.4 mm) with a weight of only 77 g. Servos of this type require a pulse width modulated (PWM) digital signal to control commanded position, but benefit from having internal, hard wired, closed loop control systems.

Commanding the position of the servo motor is equivalent to commanding a rotation angle of the spooling pulley, which is defined as δ_p, and therefore this is the primary variable which describes the deflected state of the FishBAC airfoil. It is important to note that since the kinematics of the spooling pulley and tendon mechanism are fundamentally different from the rotation of a flap, the magnitudes of the two deflection variables (namely δ_f and δ_p) are not directly comparable. It is more meaningful instead to compare the flap and FishBAC in terms of lift coefficient generated from the different deflection schemes, as will be done below.

While other work with compliant camber change mechanisms considers camber change in terms of the deflection of the trailing edge (either as an equivalent flap angle or as a tip displacement),[13] the amount of deflection seen in a compliant system such as this depends on both actuator setting and aerodynamic pressure loading, which changes across a given test. While the elastic deformations of the airfoil are indeed important (as work to be published will show)[20] it is simpler and more consistent for the sake of this wind tunnel test to describe the deflected state of the FishBAC purely in terms of the actuator input, as this is held constant during a given test.

Figure 2 shows the FishBAC prototype as built. Figure 2a shows the airfoil at rest (δ_p = 0°) while Figure 2 shows the largest camber deflections tested in this experiment, with δ_p = 90°. In this case, 36 mm of vertical tip displacement is achieved, which is 12% of the chord. Note that the limiting factor for achievable deflections was the torque available from the servo motor.

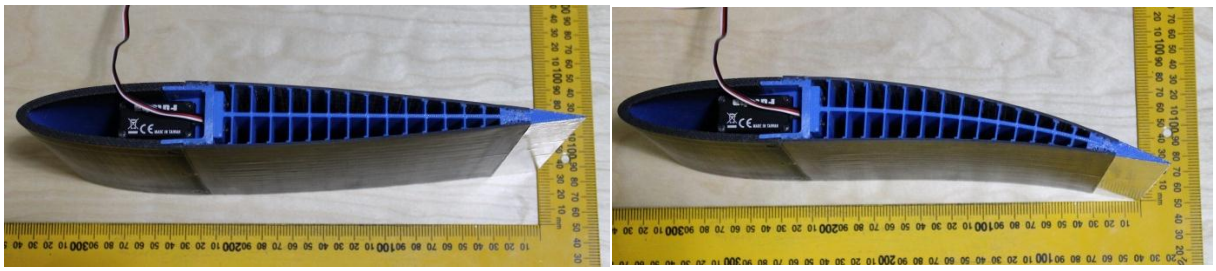

(a) (b)

Figure 2. FishBAC wind tunnel model, (a) baseline state (δ_p = 0°) and (b) deflected with δ_p = 90°

3.2. Flapped Airfoil Wind Tunnel Model Construction

The flapped airfoil model consisted of a 305 mm chord NACA 0012 airfoil with a 25% chord plain flap. The wind tunnel test model was designed to create a purely two-dimensional flapped geometry. To this end there were no control horns, flap tracks, or any other protuberances into the flow. Additionally, the gap between the flap and airfoil was sealed to maximize the increase in lift and minimize the increase in drag due to flap deflection.[21,22] This model therefore represents a best case scenario for the flap as it omits sources of additional drag which would likely be present in implementation. The airfoil geometry was printed out of ABS plastic on the same machine as the FishBAC airfoil section. The flap was attached to the main body of the airfoil via two 5 mm indexing pins. These pins also set the angle of the flap via a symmetric series of twenty spaced holes, with each pair of holes establishing a flap deflection angle (as defined in Figure 3a) of δ_f = 0° to δ_f = 45° in 5° increments. Figure 3a shows a design schematic view of the airfoil, and Figure 3b shows the model as built.

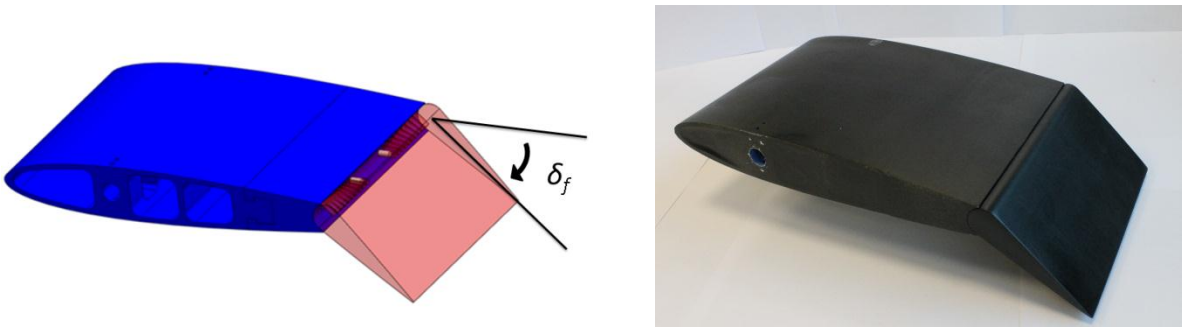

(a) (b)

Figure 3. Flapped airfoil wind tunnel model, (a) angle indexing mechanism, and (b) as built.

3.3. Wind Tunnel Setup and Test Parameters

The aerodynamic experiments were conducted in a fully automated, low speed, open circuit, and closed test section wind tunnel.[23] At the inlet, an aluminum honeycomb flow-straightener and a fiberglass mesh are used to condition the flow. Flow velocity during the tests is observed using four static pressure ports at the inlet of the test section. The test section was converted to a 610 mm by 152 mm rectangular cross section for two-dimensional experiments with the use of two removable splitter plates, as shown in Figure 4.

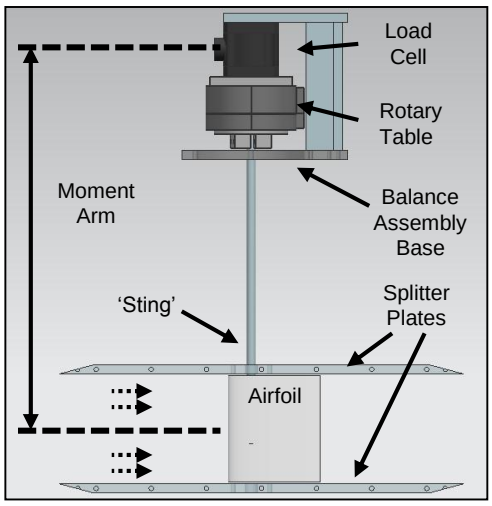

Figure 4. The wind tunnel experimental setup. Note that the upper and lower walls of the test-section and fairing around the sting are omitted.

All test parameters are controlled and measured automatically with a National Instruments (NI) cDAQ data acquisition system and a computer running NI LabVIEW software. A total of 16 channels are monitored using four NI 9239 four channel, isolated, 24-bit voltage input cards. The output signals are generated using two NI 9263 16-bit, four channel voltage output cards. For each test point, 10 seconds of data sampled at 100 Hz is averaged to get the mean value.

The streamwise turbulence of the flow in the empty test section is characterized with a standard Hot Wire Anemometry technique. The probe is placed at the center of the test section (aligned approximately at the quarter chord location along the streamwise direction) for all turbulence tests. After proper conversion of the measured voltages to velocity (V), the turbulence intensity (TI) is calculated by

$$TI = \frac{V_{rms}}{V_{mean}} \times 100 \quad (1)$$

where

$$V_{rms} = \sqrt{\frac{1}{n}\sum_{i=1}^{n}(V_i - V_{mean})^2} \quad (2)$$

and *n* is the number of sample. Turbulence intensity is measured at several velocities for different filter settings. Based on the test results, the turbulence intensity of the wind tunnel, for the 2D test section, is *TI*= 0.075%±0.01%, which is derived from 2.5 Hz-10 kHz band-pass filtered signals for the velocity range of 5-30 m/s.

For the results shown below, the tunnel wind speed was set to V = 20 m/s, which is equivalent to a Mach number of M = 0.059. The resulting chord based Reynolds number for both airfoils was therefore 390,000. Operating near a Reynolds number of 400,000 allows for the highly non-linear increases in drag that are typically seen below Re = 200,000 to be avoided,[24] and helps to reduce scatter in the data.

The commanded angle of attack was varied from α_u = -15° to α_u = 15° in 0.5° increments, where angle of attack is defined from the baseline, undeflected airfoil geometry.[22] This angle range successfully captured the onset of stall for most of the configurations tested.

It is important to note that since the span of the test models is only roughly one half of their chord, the flow environment is not expected to be purely two dimensional, even with the use of splitter plates. Three dimensional effects due to interaction between the splitter plates and test models are expected. Additionally, small gaps exist between the splitter plates and test models with this arrangement as the splitter plates are not part of the balance, and so gaps are needed to ensure that no forces are resolved into them. While made as small as possible, these gaps invariably affect the two-dimensional nature of the flow by providing a means of pressure leakage between the lower and upper surface, and by introducing additional sources of drag. For these reasons, the results presented here are not intended to be compared to other, perhaps more two-dimensional, measurements or predictions. By operating both the flapped airfoil and the FishBAC in the same flow environment a meaningful comparison can be drawn between the smooth, distributed changes in camber of the FishBAC and the sharp, discrete camber change created by the flap, even in the presence of some three-dimensional flow effects.

3.4. Tunnel Boundary Corrections

Correction factors were applied to the measured lift, drag, and moment coefficients and to the aerodynamic angles of attack to account for the effects of testing in an enclosed wind tunnel section. Specifically, the effects of body and wake blockage were accounted for using the approach outlined by Barlow, Rae, and Pope.[25] This method defines a pair of geometric parameters as

$$\sigma = \frac{\pi^2}{48}\left(\frac{c}{h}\right)^2 \tag{3}$$

$$\varepsilon = \varepsilon_{sb} + \varepsilon_{wb} = \frac{K_1 V_{model}}{C^{1.5}} + \frac{c/h}{2} C_{du} \tag{4}$$

where c is the model chord, h the test section width, K_1 is a constant approximated as K_1 = 0.52 for a model spanning the section height, V_{model} is the volume of the test model, C is the test section cross sectional area, and C_{du} is the uncorrected drag coefficient.

The impact of these parameters on angle of attack, lift, and drag coefficients are then found according to:

$$\alpha = \alpha_u + \frac{57.3\sigma}{2\pi}(C_{lu} + 4C_{mu}) \tag{5}$$

$$C_l = C_{lu}(1 - \sigma - 2\varepsilon) \tag{6}$$

$$C_d = C_{du}(1 - 3\varepsilon_{sb} - 2\varepsilon_{wb}) \tag{7}$$

where the u subscript denotes uncorrected values. These corrections are present in all the results shown below.

4. RESULTS AND DISCUSSION

The results of a measurement repeatability test will first be shown, followed by the data collected on the flapped airfoil and then data for the FishBAC airfoil. Finally, a comparison will be made between the two to show the significantly increased aerodynamic efficiency of the FishBAC.

4.1. Test Repeatability

A series of repeated tests were run with a single airfoil geometry to determine the general level of repeatability in the measured coefficients. In this case, the flapped airfoil with a flap angle setting of δ_f = 0° was swept from α_u = -15° to α_u = 15° in 0.5° increments at a commanded wind speed of 20 m/s. This test was repeated seven times. The amount of scatter in the lift and drag measurements can be considered by overlaying the lift coefficient versus drag coefficient polars for all seven runs, as shown in Figure 5. Here we can see that while there is some scatter for low magnitudes of lift coefficient ($|C_l|$ < 0.25), the repeatability of the test is generally quite good, with the measurements for all seven runs essentially lying on top of each other.

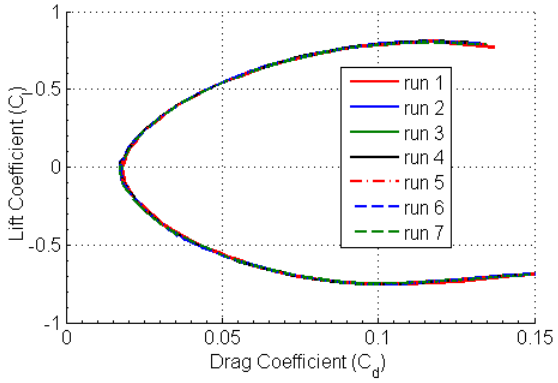

Figure 5. Test repeatability for the flapped airfoil with δ_f = 0°.

4.2. Flapped Airfoil

The effects of flap angle changes on the measured coefficients of the NACA 0012 baseline, 25% chord flapped airfoil section is discussed here.

The lift coefficient response is shown in Figure 6a for flap deflection angles between δ_f = 0° and δ_f = 30°. Above δ_f = 30° the performance was found to rapidly tail off, with very large increases in drag for minimal increases in lift, and so data from the higher deflections will not be considered here. Note in Figure 6a that the flap generally behaves as expected, and as seen in other work.[22,26] Flap deflection moves the lift curve up and to the left, resulting in an increase in lift at a given angle of attack, but also in stall occurring at progressively lower angles of attack. The flap proportionally increases lift at a given angle of attack and maximum lift coefficient, up until δ_f = 30°, where only a small lift increment is seen over δ_f = 20°. There is an interesting bubble in the lift generated with δ_f = 20° near α = 0°. The immediate cause of this is not known, but it was found to be fairly repeatable. This sharp non-linearity in the performance warrants further investigation.

The lift increment at α = 0° is ΔC_l = 0.73 when flap angle is increased from δ_f = 0° to δ_f = 30°. The maximum lift coefficient $C_{l,max}$ is 1.08 and occurs at α = 9.45° and δ_f = 30°.

It is useful to next consider the drag coefficient vs. angle of attack behavior of the flapped airfoil, as seen in Figure 6b. Here a leftwards and upwards shift can be seen in the curves due to increasing flap deflections.

By considering the lift coefficient versus drag coefficient data shown in Figure 7a (commonly referred to as the drag polar), the interplay between lift and drag can be directly seen. Here we can more clearly see the drag penalty of increasing lift by using a conventional plain flap. While increasing flap angle does indeed increase the maximum lift coefficient, it does so with a very high increase in drag. Note that the increase in zero lift drag coefficient, $\Delta C_{d,0}$ when deflecting from δ_f = 0° to δ_f = 30° is 0.054, which is 285% of the baseline $C_{d,0}$ (at δ_f = 0°).

The effect of lift and drag can be usefully combined by plotting the aerodynamic efficiency (C_l/C_d) versus angle of attack, as is done in Figure 7a. Several interesting trends appear in this data. First, note that for all flap deflection angles there is a distinct peak in the efficiency with which lift is generated. Note also that as δ_f increases, the angle of maximum efficiency decreases. For lower values of δ_f (where efficiency is highest), the aerodynamic efficiency is found to drop off quickly on either side of its maximum. This effect is less pronounced at high values of δ_f, but at the cost of

considerably lower efficiency. The overlap of the various aerodynamic efficiency curves implies that at each angle of attack there is a certain flap deflection which provides the highest efficiency. It is therefore informative to consider an "efficiency envelope", as plotted in Figure 7b, which shows the maximum operating efficiency at each angle of attack obtainable by varying δ_f. This is a useful curve for comparison between the two camber change mechanisms, as will be seen below.

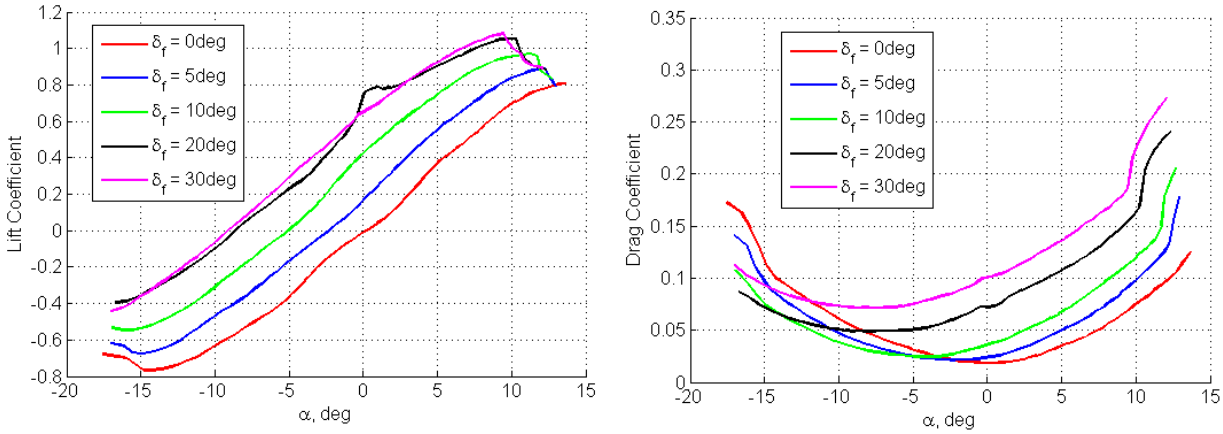

(a) (b)

Figure 6. (a) Lift and (b) drag coefficients versus angle of attack for the flapped airfoil.

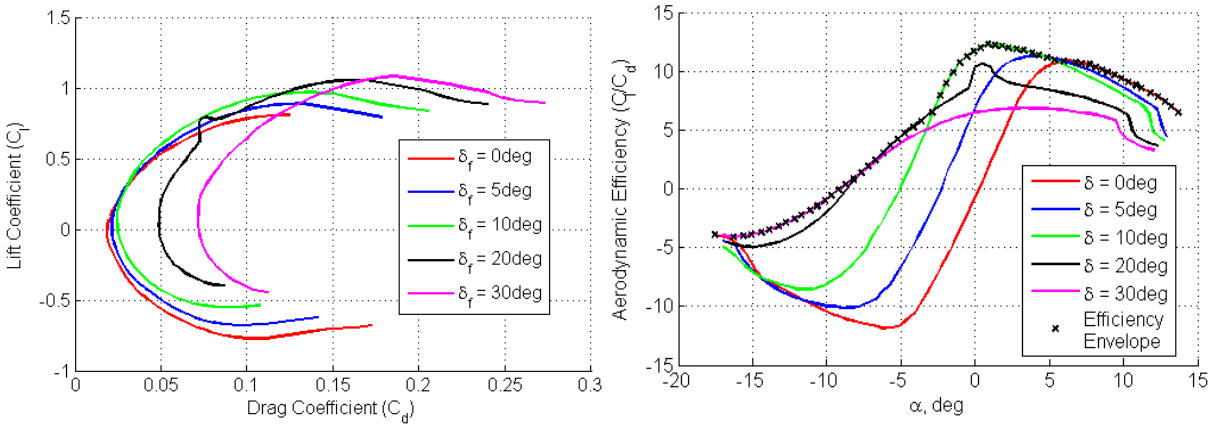

(a) (b)

Figure 7. (a) Drag polars and (b) aerodynamic efficiency versus angle of attack for the flapped airfoil

4.3. FishBAC Airfoil

The aerodynamic measurements for the Fish Bone Active Camber airfoil will be presented in a manner similar to the flapped airfoil.

The lift polars for the FishBAC airfoil can be seen in Figure 8a. Deflections of the FishBAC airfoil produce a similar effect on the lift as a flap, namely an upwards and to the left movement of the lift polars. Unlike the flap, however, there is not a tail off in the performance of the flap with higher deflections, at least not over the range of δ_p tested. This implies that trailing edge separation has been delayed. The lift increment between δ_p = 0° and δ_p = 90° at α = 0° is ΔC_l = 0.72, which is nearly identical to that achieved over the range of flap deflections tested. The maximum measured lift coefficient, $C_{l,max}$ is 1.07 and occurs at α = 8.23° and δ_p = 90°. The maximum lift coefficient is also nearly identical to that achieved by the flap, although it occurs at an angle of attack 1.2° lower than the flap. Despite the small difference in angle of maximum lift, the two variable camber mechanisms can be considered to produce similar lift behavior.

The drag coefficient versus angle of attack results for the FishBAC are shown in Figure 8b. In this case, the primary effect of increasing camber deflections is a shift to the left in the curves, with the angle of minimum drag becoming increasingly negative. Only a small net increase in drag is seen, implying the lift increase is achieved with only a small drag penalty.

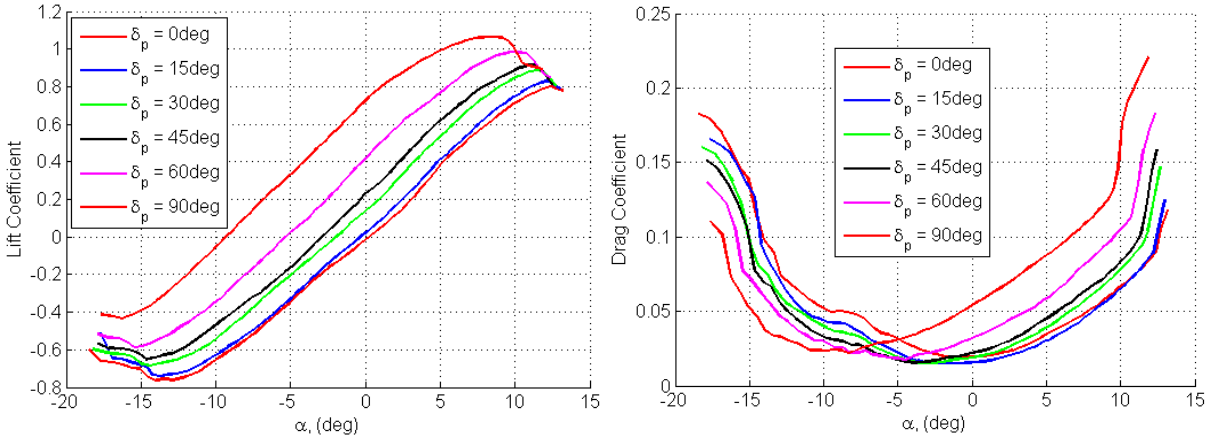

(a) (b)

Figure 8. (a) Lift and (b) drag coefficients versus angle of attack for the FishBAC airfoil.

As before, plotting the drag polars allows for simultaneous consideration of the lift and drag. Figure 9a shows that the increase in drag associated with camber change for the FishBAC is significantly less than that seen in Figure 7a for the flapped airfoil. For the FishBAC, the increase in zero lift drag coefficient, $\Delta C_{d,0}$ when deflecting from δ_p = 0° to δ_p = 90° is 0.009, which is 59% of the minimum $C_{d,0}$.

Figure 9b shows the aerodynamic efficiency of the FishBAC airfoil plotted against angle of attack. Here we see a similar behavior as in Figure 7b. Each camber deflection has an angle of attack range over which it provides the maximum obtainable efficiency. Again, the angle of attack for maximum efficiency decreases with increasing camber. The "efficiency envelope" is plotted over the individual curves to show maximum obtainable performance.

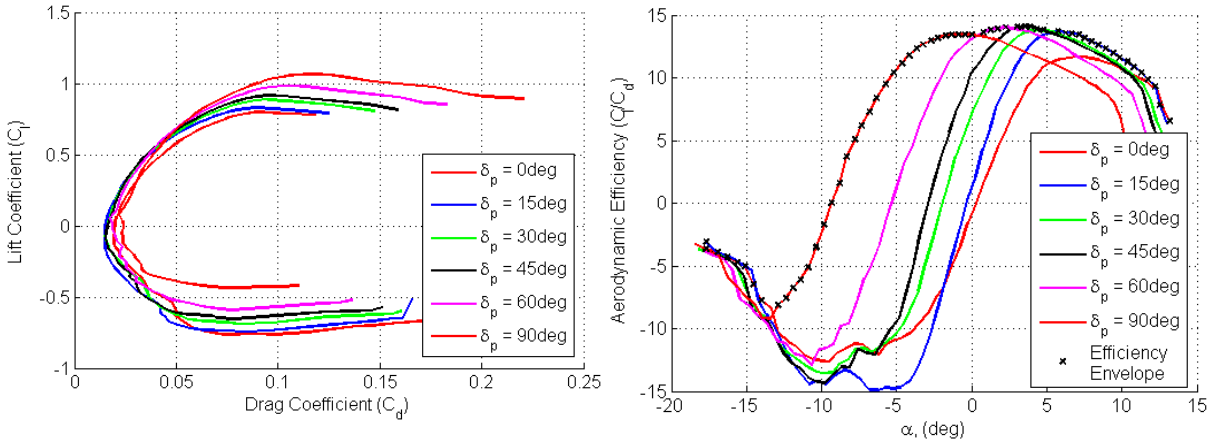

(a) (b)

Figure 9. (a) Drag polars and (b) aerodynamic efficiency versus angle of attack for the FishBAC airfoil.

4.4. Aerodynamic Efficiency Comparison

Having considered the aerodynamics of the two camber change mechanisms individually, it is also useful to compare them directly. Since the range of lift coefficients obtainable is very similar, and the Reynolds numbers are matched, the relative aerodynamic performance of the two approaches can best be seen by overlaying the "efficiency envelopes", and comparing the best obtainable performance from each device. This is done in Figure 10a, where the superior aerodynamic performance of the FishBAC can be seen. Not only does the FishBAC have significantly higher aerodynamic efficiency, it also shows less sensitivity to angle of attack. The maximum efficiency of the FishBAC has a gentle plateau, with a high level of efficiency across a broad range of angles of attack, as opposed to the more distinctly peaked behavior of the flap, which indicates a significantly smaller angle range for best performance. Quantitatively, the FishBAC is able to retain 95% of its maximum value of aerodynamic

efficiency over an angle of attack range of 9.05° (α = -1.75° to α = 7.3°), whereas the flapped airfoil has a corresponding range of only 3.6° (α = -0.1° to α = 3.5°). Note that the portion of this plot with negative aerodynamic efficiency (below α = -9.5°) is not of primary interest here, as a positively cambered airfoil would not in practice be used to create negative lift coefficients. Given the bi-directional nature of both the flapped airfoil and the FishBAC airfoil, negative lift coefficients would be more efficiently produced with negative camber.

The improvement in efficiency of the FishBAC over the flapped airfoil is quantified in Figure 10b, where it can be seen that at low lift coefficients (which correspond to negative angles of attack) the improvement is quite large. The impact of the 250% increase in efficiency obtained at α = -8° on a practical application is not necessarily significant though, as wings and blades are rarely operated at lift coefficients close to zero. Instead it is perhaps most useful to consider the angle of attack range of α = 5° to α = 10°, as this is more representative of typical operating angles in both fixed and rotary wing applications. Over this range, the FishBAC achieves roughly a 25% increase in aerodynamic efficiency, which could lead to significant improvements in the operation of all the proposed application areas, including fixed wing aircraft, helicopters, wind turbines, tidal stream turbines and tiltrotors.

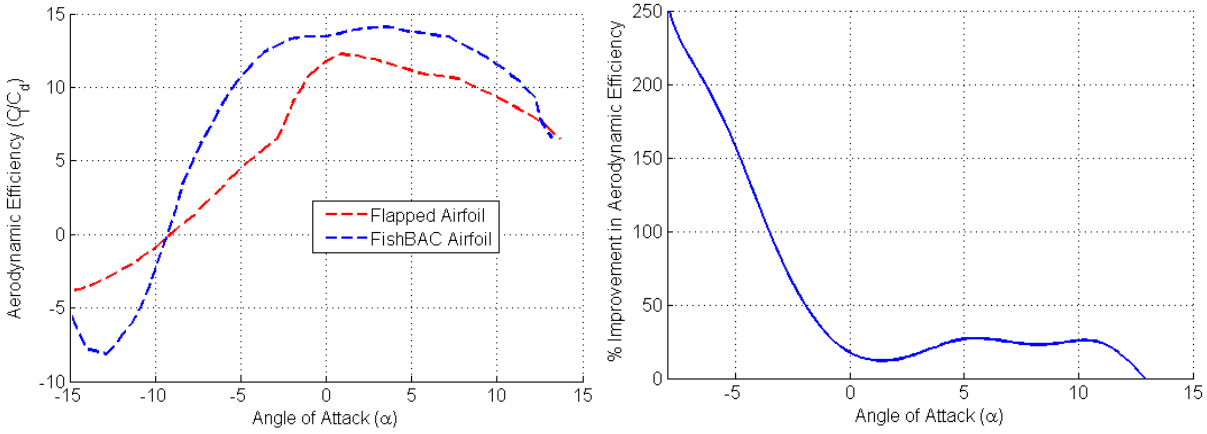

(a) (b)

Figure 10. (a) Aerodynamic efficiency envelope comparison, and (b) improvement in efficiency of the FishBAC over the flapped airfoil

5. CONCLUSIONS

This work presents wind tunnel testing of the Fish Bone Active Camber morphing concept which has been proposed as a compliant morphing structure applicable to a wide range of fixed and rotary wing applications. The concept was first introduced, with the four primary components of the design discussed. The construction of a FishBAC wind tunnel test article and a plain flapped airfoil which provides the comparison point were then detailed. The specifics of the wind tunnel used and operating conditions tested were given, after which the tunnel boundary correction equations employed were shown. A repeatability test showed very little scatter in the data for the baseline airfoil over a large number of runs. The measured aerodynamic coefficients of the two airfoils were then presented and discussed. With regard to the aerodynamic performance of the FishBAC and flapped airfoils, the following conclusions can be drawn:

1. The flapped and FishBAC airfoils are capable of similar performance in terms of the lift coefficients generated over the range of camber changes induced. For the largest deflections tested, both generate a lift increment at α = 0° of $\Delta C_l \approx 0.72$ and a maximum lift coefficient of $C_{l,max} \approx 1.07$.
2. The flapped airfoil, despite being a plain flap with a sealed gap and no external flow protuberances (such as control horns or flap tracks) shows a large increase in drag due to flap

deflection. The increase in zero lift drag coefficient, $\Delta C_{d,0}$, due to flap deflection is 0.054, which is 285% of the minimum $C_{d,0}$ (at $\delta_f = 0°$).

3. The FishBAC airfoil generates considerably less drag while generating similar levels of lift. The increase in zero lift drag coefficient, $\Delta C_{d,0}$, due to FishBAC camber change is 0.009, which is 59% of the minimum $C_{d,0}$.
4. The aerodynamic efficiency of the FishBAC airfoil is less sensitive to angle of attack, displaying a broad plateau of high efficiency as opposed to the distinct peak seen with the flapped airfoil. The FishBAC retains 95% of its maximum aerodynamic efficiency over an angle of attack range of 9.05° (α = -1.75° to α = 7.3°), whereas the flapped airfoil has a corresponding range of only 3.6° (α = -0.1° to α = 3.5°).
5. The FishBAC morphing airfoil shows a noteworthy increase in aerodynamic efficiency of roughly 25% compared to the flapped airfoil over the range of angles of attack typical of fixed wing and rotary wing applications.

Acknowledgments

The research leading to these results has received funding from the European Research Council under the European Union's Seventh Framework Programme (FP/2007-2013) / ERC Grant Agreement n. [247045].

References

[1] Abzug, M.J., and Larrabee, E.E., *Airplane Stability and Control, Second Edition; A History of the Technologies That Made Aviation Possible*, Cambridge University Press, Cambridge, UK, 2002, pg. 3.

[2] Raymer, D.P., *Aircraft Design: A Conceptual Approach*, AIAA, Washington, D.C., 1992.

[3] Kaman, C.H., "Aircraft of Rotary Wing Type," U.S. Patent No. 2,455,866, filed August 19, 1946, issued December 7, 1948.

[4] Overgaard. O., and Livingston, J., "Recent Development of the Ship Rudder with Particular Reference to the 'Flettner Rudder'," *Trans. Soc. Naval Arch. And Marine Eng*., Vol. 34, 1926, pg. 205.

[5] Burcher, R., and Rydill, L., *Concepts in Submarine Design*, Cambridge University Press, Cambridge, England, 1995.

[6] Shinners, S., *Modern Control System Theory and Design*, John Wiley & Sons, Inc, New York, NY, 1998, pp. 22-23.

[7] Chopra, I, "Review of State of Art of Smart Structures and Integrated Systems," *AIAA Journal*, 2002, 40:2145-2187.

[8] Giurgiutiu, V., "Recent Advances in Smart-Material Rotor Control Actuation," Proceedings of the AIAA/ASME/ASCE/AHS/ASC 41st Structures, Structural Dynamics and Materials Conference, AIAA-2000-1709, Atlanta, GA, April 3-6 2000.

[9] Grohmann, B., Maucher, C., Prunhuber, T., Janker, P., Dieterich, O., Enenkl, B., Bauer, M., Ahci, E., Altmikus, A., Baier, H., "Multidisciplinary Design and Optimization of Active Trailing Edge for Smart Helicopter Rotor Blade," *Mechanics of Advanced Materials and Structures*, 2008, Vol. 15, No. 3, 307-324.

[10] Antoni, U., "Construction of Flexible Aeroplane Wings Having a Variable Profile," US Patent No. 1,886,362, filed August 24, 1931, issued November 8, 1932.

[11] Barbarino, S., Bilgen, O., Ajaj, R.M., Friswell, M.I., Inman, D.J., "A Review of Morphing Aircraft," *Journal of Intelligent Material Systems and Structures*, June 2011, Vol. 22, No. 9 pp. 823-877.

[12] Bartley-Cho, J.D., Wang, D.P., Martin, C.A., Kudva, J.N., and West M.N., "Development of high-rate, adaptive trailing edge control surface for the smart wing phase 2 wind tunnel model". *Journal of Intelligent Material Systems and Structures* 2004, 15: 279–291.

[13] Daynes, S., and Weaver, P.M., "Morphing Blade Fluid-Structure Interaction", Proceedings of the 53rd AIAA/ASME/ASCE/AHS/ASC Structures, Structural Dynamics, and Materials Conference, 2012.

[14] Woods, B.K.S., and Friswell, M.I., "Preliminary Investigation of a Fishbone Active Camber Concept," Proceedings of the ASME 2012 Conference on Smart Materials, Adaptive Structures and Intelligent Systems, September 19-21, 2012, Stone Mountain, GA.

[15] Bubert, E.A., Woods, B.K.S., Lee, K., Kothera, C.S., and Wereley, N.M., "Design and Fabrication of a Passive 1D Morphing Aircraft Skin," *Journal of Intelligent Material Systems and Structures*, April 2010, Vol. 21, No. 17, pp. 1699-1717. DOI: 10.1177/1045389X10378777

[16] Murray, G., Gandhi, F., and Bakis, C., "Flexible Matrix Composite Skins for One-dimensional Wing Morphing," *Journal of Intelligent Material Systems and Structures*, April 2010, Vol. 21, No. 17, pp. 1771-1781. DOI: 10.1177/1045389X10369719

[17] Woods, B.K.S., Wereley, N.M., and Kothera, C.S., "Wind Tunnel Testing of a Helicopter Rotor Trailing Edge Flap Actuated via Pneumatic Artificial Muscles," *Journal of Intelligent Material Systems and Structures*, 2011, Vol. 22, No. 13, pp. 1513:1528. DOI: 10.1177/1045389X11424216

[18] Leishman, J. *Principles of Helicopter Aerodynamics*, Cambridge University Press, New York, 2000.

[19] Vocke, R.D., Kothera, C.S., Woods, B.K.S. and Wereley, N.M., "Development and Testing of a Span-Extending Morphing Wing," *Journal of Intelligent Material Systems and Structures*, July 2011, Vol. 22, No. 9, pp. 879-890. DOI: 10.1177/1045389X11411121

[20] Woods, B.K.S., and Friswell, M.I., "Fluid-Structure Interaction Analysis of the Fish Bone Active Camber Mechanism," To be presented at the 54th AIAA Structures, Structural Dynamics, and Materials Conference, Boston, MA, April 8-11, 2013.

[21] Riebe, J., and Church, O., "Wind-Tunnel Investigation of Control-Surface Characteristics, XXI – Medium and Large Aerodynamic Balances of Two Nose Shapes and a Plain Overhang Used with a 0.40-Airfoil-Chord Flap on an NACA 0009 Airfoil," NACA Advance Restricted Report L5C01, Langley Field, VA., March 1945.

[22] Abbott, I., and Von Doenhoff, A., *Theory of Wing Sections*, Dover Publications, New York, 1958, pp. 190-197.

[23] Bilgen, O., Friswell, M.I., "Implementation of a Continuous-Inextensible-Surface Piezocomposite Airfoil," *Journal of Aircraft*, in press, 2012.

[24] Selig. M.S., and McGranahan, B.D., "Wind Tunnel Aerodynamic Tests of Six Airfoils for Use on Small Wind Turbines," *Journal of Solar Energy Engineering*, November 2004, Vol. 126, No. 4, pg. 986. DOI: 10.1115/1.1793208

[25] Barlow, J.B., Rae, W.H. Jr., Pope, A., *Low-Speed Wind Tunnel Testing*, 3rd ed., John Wiley & Sons, New York, NY, 1999.

[26] Jacobs, E., and Pinkerton, R. 1931. "Pressure Distribution Over a Symmetrical Airfoil Section with Trailing Edge Flap," NACA Technical Report No. 360.